Analysis of Multi-Body Nonlinear Dynamic Modeling and Motion Characteristics of Flexible-Wing Aircraft

Hao Zhang, Zi-li Chen, Jingang Qiu
Unmanned Aerial Vehicle Engineering Department
Mechanical Engineering College
050003 Shijiazhuang
China
Email:zhanghao6681@sina.com

Abstract:- Flexible-wing aircraft has more applications than traditional parafoil system for its superior flight performance and height controllability. In consideration of the apparent mass of parafoil and the relative motion between two bodies, an eight degrees of freedom (DOF) nonlinear dynamic model is proposed against the special structure of two-point flexible connection of the flexible-wing aircraft, including six DOF of parafoil and two relative motion DOF of payload. The simulation emphasizes on the analysis of the model's relative motion of turning, flare landing and responses to thrust and wind disturbances. The result shows the flexible-wing aircraft is subjective to wind disturbance and the control may cause varying degrees of relative motion between two bodies, thereby further verifying model correctness and applicability.

Key-Words: -Flexible-wing aircraft; Multi-body; Nonlinear dynamic; Relative motion； Wind disturbances

1 Introduction

Flexible-wing aircraft has gradually become a research hotspot in the new unmanned aircraft field for its excellent flight performance and application advantages in material delivery, reconnaissance and surveillance in recent years[1]. The flexible-wing aircraft is consists of traditional parafoil and power plant that equipped on the back of payload unit so as to add height and velocity controllability, attitude flexibility, and improve application space while keeping basic functions of the traditional parafoil.

Some modeling analysis methods against this system have been proposed both at home and abroad. The research [2-5] on dynamic model of traditional parafoil system mainly focuses on six DOF. The parafoil and payload were regarded as rigid connection. The translational motion and rotational motion of mass center of the whole system were studied. [6-9] did some research on eight DOF dynamic model of unpowered parafoil system considering relative motion between parafoil and payload. In paper [6], the apparent mass of parafoil was not taken into account in the model. The research [7] improved the model of [6], and the eight DOF model with apparent mass matrix was built. In [8-9], the constraint forces and

moments were found in the established model, and the responses to open-loop and closed-loop turn commands were simulated and analyzed. [10] studied the longitude motion of the flexible-wing aircraft. Only considering relative pitch motion, the simplified dynamic model of four DOF was built in vertical plane. And control algorithms of the longitude motion were studied. [11] studied the flexible-wing aircraft longitudinal flight performance aiming at a simple static model, and the issue of parafoil collapse was analyzed. [12-13] built an eight DOF nonlinear dynamic model of the flexible-wing aircraft neglecting relative roll motion between two bodies, and the friction at connecting points was taken into account, conducted simulated analysis on its motion characteristics after linear processing; The existing researches mainly con- centrate on some unpowered units such as parafoil-payload drop system but only few re- searches focus on modeling of the flexible-wing aircraft, which is one of the reasons that a reasonable nonlinear control method cannot be used to correctly and effectively control it.

The parafoil is made of flexible fabric, so the apparent mass must be taken into account when flying in fluid after inflated completely. The traditional dynamic equation of rigid body has six DOF and always neglecting the effect of apparent mass. However, the multi-body structure of the flexible-wing aircraft is more complicated and the thrust and the lines deflection changes have great influence on the payload attitude when completing low-altitude and low-velocity reconnaissance, etc. Therefore, relative motion in flight change must be considered when motion characteristics of the flexible-wing aircraft are analyzed.

In this paper, on the basis of previous studies, a mechanism method is proposed to build an eight DOF nonlinear dynamic model of the flexible-wing aircraft. Regarding the parafoil and payload as single individuals, the forces acting on the two bodies are analyzed in their own coordinates. The parafoil has six DOF (translational motion with the mass center and rotational motion around the mass center), and the payload has two DOF (relative yaw motion and relative pitch motion).This paper emphasizes on the analysis of relative motion characteristics of flexible-wing aircraft, so the flight motions such as turning, flare landing and the responses to power and wind disturbances are analyzed in detail. The simulation results verify the validity of model.

This paper is organized as follows. In Sect. 2, the dynamic model of eight DOF based on a mechanism method is established. In Sect. 3, the model's relative motion of turning, flare landing and responses to power are analyzed. In Sect. 4, simulations have been carried out for the model in the presence of wind disturbances. In last section, the research work is summarized, and some existing problems are indicated.

2 Nonlinear dynamic model of system

2.1 Model characteristics and assumptions

It is necessary to conduct the following basic assumptions against model characteristics of the flexible-wing aircraft before modeling and analysis:

1) Without maneuvering, the parafoil is considered to be a fixed shape once it has

completely inflated and has two planes of symmetries;

2) The suspension lines of the parafoil are combined with the payload at two connection points, and the lines length change is neglected;

3) The payload is assumed as a rigid body with regular shape and the lift is ignored;

4) The ground is a plane.

2.2 Definition of the coordinate system

In order to facilitate analysis, three main coordinate systems are established as Fig. 1.

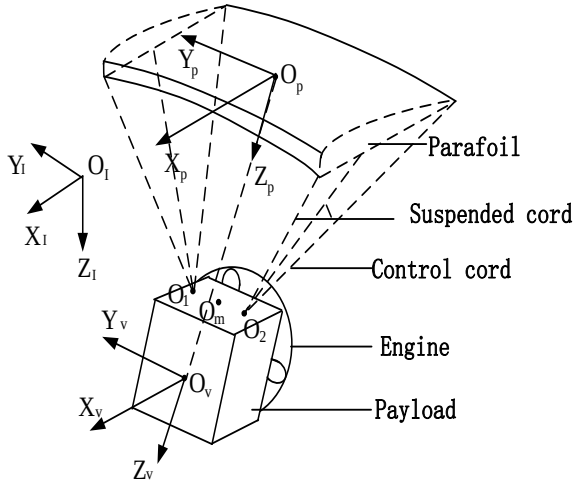

Fig. 1 Definition of coordinate system

1) The inertial coordinate system is $\Sigma_I(X_I,Y_I,Z_I)$. The plane $O_IX_IY_I$ is horizontal. The positive direction of Z_I axis is perpendicular to the horizontal plane downward, conforming to right-hand system, the location of the origin is on the earth.

2) The origin O_p of parafoil coordinate system $\Sigma_p(X_p,Y_p,Z_p)$ is chosen at the center of gravity (CG) of the parafoil and the positive direction of Z_p axis is chosen in the direction from O_p to O_m, the X_p axis perpendicular to the Z_p axis in the symmetry plane of the parafoil and the positive direction is taken forward. The Y_p axis is perpendicular to $O_pZ_pX_p$ plane, conforming to right-hand system.

3) The origin O_v of payload coordinate system $\Sigma_v(X_v,Y_v,Z_v)$ is taken at the CG of the payload and the positive direction of X_v axis is along thrust direction, the Z_v axis is downward and perpendicular to the X_v axis in the symmetry plane, and Y_v axis is perpendicular to $O_vZ_vX_v$ plane, conforming to right-hand system.

The transformation matrix from the inertial to the parafoil coordinate system is defined by three attitude angles (ϕ_p,θ_p,ψ_p) of the parafoil:

$$\mathbf{T}_{Ip}=\begin{bmatrix} c\theta_p c\psi_p & c\theta_p s\psi_p & -s\theta_p \\ s\phi_p s\theta_p c\psi_p - c\phi_p s\psi_p & s\phi_p s\theta_p s\psi_p + c\phi_p c\psi_p & s\phi_p c\theta_p \\ c\phi_p s\theta_p c\psi_p + s\phi_p s\psi_p & c\phi_p s\theta_p s\psi_p - s\phi_p c\psi_p & c\phi_p c\theta_p \end{bmatrix} \quad (1)$$

For arbitrary angle α: $\sin\alpha \equiv s\alpha$, $\cos\alpha \equiv c\alpha$.

Assuming the suspension lines length change is ignored and relative rolling motion is neglected, the transformation matrix from the payload to the parafoil coordinate system can be defined by two attitude angles (ψ_{vp},θ_{vp}) of the payload which is relative to the parafoil:

$$\mathbf{T}_{vp}=\begin{bmatrix} c\theta_{vp} c\psi_{vp} & -s\psi_{vp} & s\theta_{vp} c\psi_{vp} \\ c\theta_{vp} s\psi_{vp} & c\psi_{vp} & s\theta_{vp} s\psi_{vp} \\ -s\theta_{vp} & 0 & c\theta_{vp} \end{bmatrix} \quad (2)$$

2.3 Dynamic equation

2.3.1 Translational motion of the payload

The payload is regarded as a rigid body with regular shape in this paper, so the motion equation of payload is represented by traditional momentum and moment momentum. The force on the payload mainly include aerodynamic force $\boldsymbol{F}_{vA}$, gravity $\boldsymbol{F}_{vG}$, inertial force $\boldsymbol{F}_{vI}$, tension of suspension lines $\boldsymbol{F}_{vT}$, and thrust $\boldsymbol{F}_{vth}$, and these forces satisfy Eq. (3):

$$\boldsymbol{F}_{vA}+\boldsymbol{F}_{vG}+\boldsymbol{F}_{vI}+\boldsymbol{F}_{vT}+\boldsymbol{F}_{vth}=\mathbf{0}_{3\times1} \quad (3)$$

1) The aerodynamic force $\boldsymbol{F}_{vA}$ is given by:

$$\boldsymbol{F}_{vA}=\frac{1}{2}\rho V_v^2 S_v C_{Dv}\boldsymbol{T}_{vp}\begin{pmatrix}\cos\alpha_v\cos\beta_v\\ \sin\beta_v\\ \sin\alpha_v\cos\beta_v\end{pmatrix} \tag{4}$$

where ρ denotes the atmospheric density, $V_v=\sqrt{u_v^2+v_v^2+w_v^2}$, S_v denotes the reference area of the payload, the lift is ignored, attack angle of the payload $\alpha_v=\tan^{-1}(w_v/u_v)$, the sideslip angle $\beta_v=\sin^{-1}(v_v/V_v)$, C_{Dv} denotes the drag coefficient.

2) The gravity $\boldsymbol{F}_{vG}$ is given by:

$$\boldsymbol{F}_{vG}=m_v g\begin{pmatrix}-\sin\theta_p\\ \cos\theta_p\sin\phi_p\\ \cos\theta_p\cos\phi_p\end{pmatrix} \tag{5}$$

where m_v denotes the mass of the payload.

3) The inertial force $\boldsymbol{F}_{vI}$ is given by:

$$\boldsymbol{F}_{vI}=-m_v\boldsymbol{A}_{vp} \tag{6}$$

where $\boldsymbol{A}_{vp}$ is the acceleration of the payload in parafoil coordinate[13].

4) The thrust $\boldsymbol{F}_{vth}$ acts to the CG of the payload along the X_v axis, which is given by:

$$\boldsymbol{F}_{vth}=\boldsymbol{T}_{vp}\begin{bmatrix}F_{vthX} & 0 & 0\end{bmatrix}^{\mathrm{T}} \tag{7}$$

All of the above equations are substituted into Eq. (3), the equation can then be written as:

$$\boldsymbol{E}_{Fv}\dot{\boldsymbol{x}}=-(\boldsymbol{F}_{vA}+\boldsymbol{F}_{vG}+\boldsymbol{F}_{vT}+\boldsymbol{F}_{vth}+m_v\boldsymbol{L}_{p1}+m_v\boldsymbol{L}_{v3}) \tag{8}$$

where $\boldsymbol{x}=[\boldsymbol{V}_p^{\mathrm{T}}\ \boldsymbol{\omega}_p^{\mathrm{T}}\ \boldsymbol{\omega}_{\mathrm{vp}}^{\mathrm{T}}\ \theta_{vp}\ \psi_{vp}\ \phi_p\ \theta_p]^{\mathrm{T}}$,and $\boldsymbol{V}_p=[u_p\quad v_p\quad w_p]^T$, $\boldsymbol{\omega}_p=[p_p\quad q_p\quad r_p]^{\mathrm{T}}$, $\boldsymbol{\omega}_{\mathrm{vp}}=[q_{vp}\quad r_{vp}]^{\mathrm{T}}$, and $\boldsymbol{E}_{Fv}=m_v\begin{bmatrix}\boldsymbol{I}_3 & \boldsymbol{L}_{v1} & \boldsymbol{L}_{v2} & \boldsymbol{0}_{3\times4}\end{bmatrix}$, and $\boldsymbol{L}_{p1}$, $\boldsymbol{L}_{v3}$, $\boldsymbol{L}_{v1}$, and $\boldsymbol{L}_{v2}$ denote matrix variables of $\boldsymbol{\omega}_p$, $\boldsymbol{\omega}_{vp}$, θ_{vp}, and ψ_{vp}.

2.3.2 Rotational motion of payload

The moment due to gravity and the thrust are zero, since the forces act in the CG of the payload. The moments about the CG includes aerodynamic moment $\boldsymbol{M}_{vA}$, inertial moment $\boldsymbol{M}_{vI}$, and tension moment $\boldsymbol{M}_{vT}$, these moments satisfy Eq. (9):

$$\boldsymbol{M}_{vA}+\boldsymbol{M}_{vI}+\boldsymbol{M}_{vT}=\boldsymbol{0}_{3\times1} \tag{9}$$

1) We assume that $\boldsymbol{M}_{vA}$ is only the pitch moment, and is given by:

$$\boldsymbol{M}_{vA}=\frac{1}{2}\rho V_v^2 S_v c_v\begin{bmatrix}0 & C_{mv}+k_{pv}C_{mqv}q_v & 0\end{bmatrix}^{\mathrm{T}} \tag{10}$$

where c_v is the reference length of the payload along X_v axis, $k_{pv}=c_v/(2u_p)$, C_{mv} and C_{mqv} are aerodynamic derivative coefficients of the payload.

2) We assume that the payload is a rigid body and has two planes of symmetry, then $I_{XYv}=I_{YZv}=I_{ZXv}=0$, the inertial moment $\boldsymbol{M}_{vI}$, is given by:

$$\boldsymbol{M}_{vI}=-\boldsymbol{J}_{vI}\dot{\boldsymbol{\omega}}_v+\boldsymbol{M}_{vI1} \tag{11}$$

where

$$\begin{aligned}\boldsymbol{J}_{vI}&=\begin{bmatrix}I_{Xv}&0&0\\0&I_{Yv}&0\\0&0&I_{Zv}\end{bmatrix}\\ \boldsymbol{M}_{vI1}&=\begin{bmatrix}0&I_{Zv}-I_{Yv}&0\\0&0&I_{Xv}-I_{Zv}\\I_{Yv}-I_{Xv}&0&0\end{bmatrix}\begin{bmatrix}p_vq_v\\q_vr_v\\p_vr_v\end{bmatrix}\end{aligned} \tag{12}$$

The angular velocity of the payload $\boldsymbol{\omega}_v$ in is given by:

$$\boldsymbol{\omega}_v=\begin{bmatrix}0 & q_{vp} & 0\end{bmatrix}^{\mathrm{T}}+\boldsymbol{T}_{vp}^{-1}\left(\omega_p+\begin{bmatrix}0 & 0 & r_{vp}\end{bmatrix}^{\mathrm{T}}\right) \tag{13}$$

Differentiating Eq. (13) and using the relation $\boldsymbol{T}_{vp}^T=\boldsymbol{T}_{vp}^{-1}$:

$$\dot{\boldsymbol{\omega}}_v=\boldsymbol{T}_{vp}^T\dot{\boldsymbol{\omega}}_p+\boldsymbol{\Omega}_{v1}\dot{\boldsymbol{\omega}}_{vp}+\boldsymbol{\Omega}_{v2} \tag{14}$$

where

$$\boldsymbol{\Omega}_{v1}=\begin{bmatrix}0&-\sin\theta_{vp}\\1&0\\0&\cos\theta_{vp}\end{bmatrix},\quad \boldsymbol{\Omega}_{v2}=\dot{\boldsymbol{T}}_{vp}^T\begin{bmatrix}p_v\\q_v\\r_p+r_{vp}\end{bmatrix}.$$

3) The tension moment $\boldsymbol{M}_{vT}$ is:

$$\boldsymbol{M}_{vT} = [\boldsymbol{L}_{vT1} \quad \boldsymbol{L}_{vT2}][\boldsymbol{F}_{vT1}^{T} \quad \boldsymbol{F}_{vT2}^{T}]^{T} \tag{15}$$

where $\boldsymbol{F}_{vTR}$ and $\boldsymbol{F}_{vTL}$ are the tensions of parafoil suspension lines at the point O_1 and O_2, respectively, the collective tension $\boldsymbol{F}_{vT1} = \boldsymbol{F}_{vTR} + \boldsymbol{F}_{vTL}$ and the differential one $\boldsymbol{F}_{vT2} = \boldsymbol{F}_{vTR} - \boldsymbol{F}_{vTL}$, and the distance between O_1 and O_2 b_v, then:

$$\boldsymbol{L}_{vT1} = l_v \begin{bmatrix} 0 & 1 & 0 \\ -1 & 0 & 0 \\ 0 & 0 & 0 \end{bmatrix} \quad \boldsymbol{L}_{vT2} = \frac{b_v}{2} \begin{bmatrix} 0 & 0 & 1 \\ 0 & 0 & 0 \\ 1 & 0 & 0 \end{bmatrix}$$

All of the following equations are substituted into equation (9), so as to gain:

$$\boldsymbol{E}_{Mv}\dot{\boldsymbol{x}} = -(\boldsymbol{M}_{vA} + \boldsymbol{M}_{vI1} + \boldsymbol{M}_{vT} + \boldsymbol{J}_{vI}\boldsymbol{\Omega}_{v2}) \tag{16}$$

where $\boldsymbol{E}_{Mv} = \lfloor \boldsymbol{0}_{3\times3} \quad \boldsymbol{J}_{vI}\boldsymbol{T}_{vp}^{\mathrm{T}} \quad \boldsymbol{J}_{vI}\boldsymbol{\Omega}_{v1} \quad \boldsymbol{0}_{3\times4} \rfloor$.

2.3.3 Translational motion of parafoil

After having been inflated completely, the force on the parafoil mainly include gravity $\boldsymbol{F}_{pG}$, aerodynamic force $\boldsymbol{F}_{pA}$, inertial force $\boldsymbol{F}_{pI}$, and the tension $\boldsymbol{F}_{pT}$ of suspension lines, and these forces satisfy Eq. (17):

$$\boldsymbol{F}_{pG} + \boldsymbol{F}_{pA} + \boldsymbol{F}_{pI} + \boldsymbol{F}_{pT} = \boldsymbol{0}_{3\times1} \tag{17}$$

Each force is calculated as follows:

1) The gravity $\boldsymbol{F}_{pG}$ is given by:

$$\boldsymbol{F}_{pG} = m_p g[-\sin\theta_p \quad \cos\theta_p \sin\phi_p \quad \cos\theta_p \cos\phi_p]^{\mathrm{T}} \tag{18}$$

where m_p denotes the mass of the parafoil and inner air.

2) Aerodynamic force $\boldsymbol{F}_{pA}$ of the parafoil includes $\boldsymbol{F}_{pAR}$, which consists of lift, drag force, $\boldsymbol{F}_{pAM}$ by apparent mass, and $\boldsymbol{F}_{pA\delta}$ by brake deflections, which is given by:

$$\boldsymbol{F}_{pA} = \boldsymbol{F}_{pAR} + \boldsymbol{F}_{pAM} + \boldsymbol{F}_{pA\delta} \tag{19}$$

The method of segmenting treatment is used for calculating the aerodynamic force of the parafoil, which was presented by [14]. The parafoil is divided into eight distributed segments geometrically along the span-wise direction, shown as Fig. 2. Aerodynamic forces of all pieces are respectively calculated and, then, the total aerodynamic force of the parafoil can be obtained by the aerodynamic forces of eight segments.

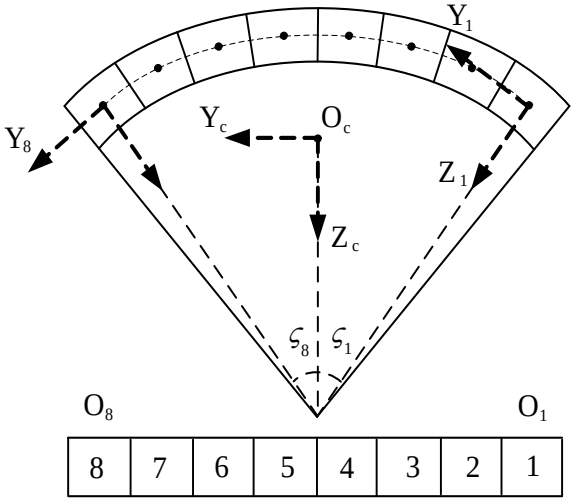

Fig. 2 The front view of segmenting of parafoil

The equations of lift and drag can be represented as follow:

$$\boldsymbol{F}_{L_i} = k_i C_{Li}(0.5\rho S_{ci}\sqrt{u_i^2 + w_i^2})[w_i \;\; 0 \;\; -u_i]^{\mathrm{T}} \tag{20}$$

$$\boldsymbol{F}_{D_i} = -C_{Di}(0.5\rho S_i V_i)[w_i \;\; 0 \;\; -u_i]^{\mathrm{T}} \tag{21}$$

where k_i denotes the product factor, ($k_1, k_8 = 0.6$, $k_2, k_7 = 1.0$, $k_3, k_6 = 1.16$, $k_4, k_5 = 1.24$), S_{ci} denotes piece area; C_{Li} and C_{Di} are lift and drag coefficients.

The total aerodynamic force $\boldsymbol{F}_{pAR}$ is given by:

$$\boldsymbol{F}_{pAR} = \sum_{i=1}^{8} \boldsymbol{T}_{i-\mathrm{O}_c}(\boldsymbol{F}_{L_i} + \boldsymbol{F}_{D_i}) \tag{22}$$

where $\boldsymbol{T}_{i-\mathrm{O}_c}$ denotes the transformation matrix of the *i* local coordinate system to the parafoil coordinate system, expressed by the angle between the lines and central axis, ς_i, its expression is:

$$\boldsymbol{T}_{i-\mathrm{O}_c}=\begin{bmatrix}1 & 0 & 0\\ 0 & \cos\varsigma_i & \sin\varsigma_i\\ 0 & -\sin\varsigma_i & \cos\varsigma_i\end{bmatrix} \tag{23}$$

The aerodynamic force due to apparent mass $\boldsymbol{F}_{pAM}$ is given by:

$$\boldsymbol{F}_{pAM}=\boldsymbol{M}_a\dot{\boldsymbol{V}}_p \tag{24}$$

where M_a denotes the apparent mass, which is calculated according to the method proposed by [15].

The aerodynamic force due to brake deflect-tions $\boldsymbol{F}_{pA\delta}$ is given by:

$$\begin{aligned}\boldsymbol{F}_{pA\delta}=&F_{dypc}S_pC_{B\delta}\delta_e\begin{bmatrix}\sin\alpha_p\\ 0\\ -\cos\alpha_p\end{bmatrix}+F_{dypc}S_pC_{B\delta}\delta_r\begin{bmatrix}0\\ 1\\ 0\end{bmatrix}\\ &+F_{dypc}S_pC_{B\delta}\delta_e\begin{bmatrix}-\cos\alpha_p\cos\beta_p\\ -\sin\beta_p\\ -\sin\alpha_p\cos\beta_p\end{bmatrix}\end{aligned} \tag{25}$$

where $F_{dypc}=0.5\rho V_p^2$, $V_p=\sqrt{u_p^2+v_p^2+w_p^2}$, and S_p denotes the reference area of the parafoil, $C_{B\delta}$, $C_{B\delta}$, and $C_{B\delta}$ are aerodynamic derivative coefficients, α_p and β_p are attack angle and sideslip angle of the parafoil, $\delta_e=\delta_R+\delta_L$ and $\delta_r=\delta_R-\delta_L$ are defined, respectively , where δ_L and δ_R are deflection of left and right brakes of the parafoil, respectively.

3) The inertial force $\boldsymbol{F}_{pI}$ is given by:

$$\boldsymbol{F}_{pI}=m_p\dot{\boldsymbol{V}}_p \tag{26}$$

All of the above equations are substituted into Eq. (17), the equation can then be written as:

$$\boldsymbol{E}_{Fp}\dot{\boldsymbol{x}}=-(\boldsymbol{F}_{pG}+\boldsymbol{F}_{pAR}+\boldsymbol{F}_{pA\delta}+\boldsymbol{F}_{pT}) \tag{27}$$

Where $\boldsymbol{E}_{Fp}=\lfloor(m_p\boldsymbol{I}_3+\boldsymbol{M}_a)\quad\boldsymbol{0}_{3\times9}\rfloor$.

2.3.4 Rotational motion of parafoil

The moments about the CG of the parafoil mainly includes the aerodynamic moment $\boldsymbol{M}_{pA}$, the inertial moment $\boldsymbol{M}_{pI}$, and the tension moment $\boldsymbol{M}_{pT}$, these moments expressed in Σ_p satisfy Eq. (28):

$$\boldsymbol{M}_{pA}+\boldsymbol{M}_{pI}+\boldsymbol{M}_{pT}=\boldsymbol{0}_{3\times1} \tag{28}$$

Each moment is calculated as follows:

1) The aerodynamic moment $\boldsymbol{M}_{pA}$ is composed of three parts ($\boldsymbol{M}_{pAR}$ by the parafoil and inner air, $\boldsymbol{M}_{pAM}$ due to apparent mass, and $\boldsymbol{M}_{pA\delta}$ by brake deflections), the aerodynamic moment is then given by the following equation:

$$\boldsymbol{M}_{pA}=\boldsymbol{M}_{pAR}-\boldsymbol{M}_{pAM}+\boldsymbol{M}_{pA\delta} \tag{29}$$

The local aerodynamic moment $\boldsymbol{M}_{pAR}$ is:

$$\boldsymbol{M}_{pAR}=\sum_{i=1}^{8}\boldsymbol{L}_{O_c}\times\boldsymbol{T}_{i-\mathrm{O}_c}(\boldsymbol{F}_{L_i}+\boldsymbol{F}_{D_i}) \tag{30}$$

where $\boldsymbol{L}_{O_c}$ denotes the position vector of the origin of local coordinate O_c in the parafoil coordinate system.

The apparent mass moment $\boldsymbol{M}_{pAM}$ is:

$$\boldsymbol{M}_{pAM}=\boldsymbol{J}_p\dot{\boldsymbol{\omega}}_p \tag{31}$$

where $\boldsymbol{J}_p$ denotes the inertia matrix of apparent mass during turning [16].

The aerodynamic force $\boldsymbol{M}_{pA\delta}$ by brake deflections is given by:

$$\boldsymbol{M}_{pA\delta}=\frac{1}{2}\rho V_p^2S_p\{b\delta_e[0\ C_{M\delta}\ 0]^{\mathrm{T}}+c\delta_a[C_{R\delta}\ 0\ C_{N\delta}]^{\mathrm{T}}\} \tag{32}$$

where b denotes the span, c denotes the chord length, $C_{M\delta}$, $C_{R\delta}$, and $C_{N\delta}$ are aerodynamic derivative coefficient.

2) The inertial moment $\boldsymbol{M}_{pI}$ is given by:

$$\boldsymbol{M}_{pI}=-\boldsymbol{J}_{pI}\dot{\boldsymbol{\omega}}_p+\boldsymbol{M}_{pI1} \tag{33}$$

where $\boldsymbol{J}_{pI}$ and $\boldsymbol{M}_{pI1}$ are represented by the moment and the product of inertial of parafoil and $\boldsymbol{\omega}_p$, as in the same way as $\boldsymbol{J}_{vI}$ and $\boldsymbol{M}_{vI1}$ in Eq. (12).

3) Similarly to $\boldsymbol{M}_{vT}$, $\boldsymbol{M}_{pT}$ is given by:

$$\boldsymbol{M}_{pT} = [\boldsymbol{L}_{pT1} \quad \boldsymbol{L}_{pT2}][\boldsymbol{F}_{vT1}^{T} \quad \boldsymbol{F}_{vT2}^{T}]^{T} \tag{34}$$

where $\boldsymbol{L}_{pT1} = \boldsymbol{L}_{pT1p}\boldsymbol{T}_{vp}$ and $\boldsymbol{L}_{pT2} = \boldsymbol{L}_{pT2p}\boldsymbol{T}_{vp}$, i.e.,

$$\boldsymbol{L}_{pT1p} = l_p \begin{bmatrix} 0 & 1 & 0 \\ -1 & 0 & 0 \\ 0 & 0 & 0 \end{bmatrix}$$

$$\boldsymbol{L}_{pT2p} = \frac{b_v}{2} \begin{bmatrix} 0 & 0 & -\cos\psi_{vp} \\ 0 & 0 & -\sin\psi_{vp} \\ \cos\psi_{vp} & \sin\psi_{vp} & 0 \end{bmatrix}$$

All of the above equations are substituted into Eq. (14), the equation can then be written as:

$$\boldsymbol{E}_{Mp}\dot{\boldsymbol{x}} = -(\boldsymbol{M}_{pAR} + \boldsymbol{M}_{pA\delta} + \boldsymbol{M}_{pI1} + \boldsymbol{M}_{pT}) \tag{35}$$

where $\boldsymbol{E}_{Mp} = \begin{bmatrix} \boldsymbol{0}_{3\times3} & \boldsymbol{M}_{a4} + \boldsymbol{J}_{pI} & \boldsymbol{0}_{3\times6} \end{bmatrix}$.

2.4 Nonlinear dynamic equation

The nonlinear dynamic equation of the flexible-wing aircraft can be gained by eliminating the tension from Eqs. (3), (9), (17) and (35).

1) We can use the relation $\boldsymbol{F}_{pT} = -\boldsymbol{F}_{vT}$ to eliminate the tensions from Eq. (3) and (17), then we have:

$$\boldsymbol{E}_F\dot{\boldsymbol{x}} = -\boldsymbol{F}_1 \tag{36}$$

where

$$\begin{aligned}\boldsymbol{F}_1 = {} & \boldsymbol{F}_{pAR} + \boldsymbol{F}_{pA\delta} + \boldsymbol{F}_{pG} + m_p\boldsymbol{L}_{pI} + \boldsymbol{F}_{vA} + \boldsymbol{F}_{vG} \\ & + \boldsymbol{F}_{vth} + m_v\boldsymbol{L}_{p1} + m_v\boldsymbol{L}_{v3}\end{aligned} \tag{37}$$

$$\boldsymbol{E}_F = \boldsymbol{E}_{Fp} + \boldsymbol{E}_{Fv} \tag{38}$$

2) We define the following matrix as $\boldsymbol{K} = \begin{bmatrix} \boldsymbol{K}_1^{\mathrm{T}} & \boldsymbol{K}_2^{\mathrm{T}} \end{bmatrix}^{\mathrm{T}}$, in which:

$$\begin{aligned}\boldsymbol{K}_1 &= \begin{bmatrix} \mathrm{c}\theta_{vp}\mathrm{c}\psi_{vp} & 0 & \mathrm{s}\theta_{vp}\mathrm{c}\psi_{vp} & 1 & 0 & 0 \\ \mathrm{c}\theta_{vp}\mathrm{s}\psi_{vp} & 0 & \mathrm{s}\theta_{vp}\mathrm{s}\psi_{vp} & 0 & 1 & 0 \\ 0 & 1 & 0 & 0 & 0 & 0 \\ -\mathrm{s}\theta_{vp} & 0 & \mathrm{c}\theta_{vp} & 0 & 0 & 1 \end{bmatrix} \\ \boldsymbol{K}_2 &= \begin{bmatrix} 0 & 0 & 0 & 0 & 0 & 1 \end{bmatrix}\end{aligned} \tag{39}$$

A relational expression can be gained as follows:

$$\boldsymbol{K}_1 \begin{bmatrix} \boldsymbol{L}^{T}_{vT2} & \boldsymbol{L}^{T}_{pT2} \end{bmatrix}^{T} = \boldsymbol{0}_{4\times3} \tag{40}$$

Multiplying $\begin{bmatrix} \boldsymbol{M}_{vT} & \boldsymbol{M}_{pT} \end{bmatrix}^{T}$ by $\boldsymbol{K}_1$, we can have:

$$\begin{aligned}\boldsymbol{K}_1 \begin{bmatrix} \boldsymbol{M}_{vT} \\ \boldsymbol{M}_{pT} \end{bmatrix} &= \boldsymbol{K}_1 \left(\begin{bmatrix} \boldsymbol{L}_{vT1} \\ \boldsymbol{L}_{pT1} \end{bmatrix} \boldsymbol{F}_{vT1} + \begin{bmatrix} \boldsymbol{L}_{vT2} \\ \boldsymbol{L}_{pT2} \end{bmatrix} \boldsymbol{F}_{vT2} \right) \\ &= \boldsymbol{K}_1 \begin{bmatrix} \boldsymbol{L}_{vT1} \\ \boldsymbol{L}_{pT1} \end{bmatrix} \boldsymbol{F}_{vT1}\end{aligned} \tag{41}$$

Similarly, the following equation is obtained:

$$\boldsymbol{K}_1 \begin{bmatrix} \boldsymbol{M}_{vT} \\ \boldsymbol{M}_{pT} \end{bmatrix} = -\begin{pmatrix} 0 \\ 0 \\ 1 \end{pmatrix} \boldsymbol{T}_{vp}\boldsymbol{M}_{vT} = k_T\boldsymbol{F}_{pTZ}\psi_{vp} + c_T r_{vp} \tag{42}$$

where k_T and c_T are proportionality coefficients, $\boldsymbol{F}_{pTZ}$ is a component of the tension $\boldsymbol{F}_{pT}$ along Z_p axis.

Multiplying Eqs. (9) and (35) by $\boldsymbol{K}$ from the left side and using Eqs. (41) and (42) yield:

$$\begin{aligned}\boldsymbol{K} \begin{bmatrix} \boldsymbol{E}_{Mv} \\ \boldsymbol{E}_{Mp} \end{bmatrix} \dot{\boldsymbol{x}} = {} & \boldsymbol{K} \begin{bmatrix} -(\boldsymbol{M}_{vA} + \boldsymbol{M}_{vI1} + \boldsymbol{J}_{vI}\boldsymbol{\Omega}_{v2}) \\ -(\boldsymbol{M}_{pAR} + \boldsymbol{M}_{pAB} + \boldsymbol{M}_{pAM0} + \boldsymbol{M}_{pI1}) \end{bmatrix} \\ & + \begin{bmatrix} \boldsymbol{K}_1 \\ \boldsymbol{K}_2 \end{bmatrix} \begin{bmatrix} -\boldsymbol{M}_{vT} \\ -\boldsymbol{M}_{pT} \end{bmatrix}\end{aligned} \tag{43}$$

$\boldsymbol{K}_1$ and $\boldsymbol{K}_2$ are substituted into equation (43), so as to gain:

$$\boldsymbol{E}_M\dot{\boldsymbol{x}} = -\boldsymbol{M}_1 \tag{44}$$

where

$$\boldsymbol{E}_M = \boldsymbol{K}\begin{bmatrix} \boldsymbol{E}_{Mv}^{\mathrm{T}} & \boldsymbol{E}_{Mp}^{\mathrm{T}} \end{bmatrix}^{\mathrm{T}} - \boldsymbol{R}_M\boldsymbol{E}_{Fp} \tag{45}$$

$$\boldsymbol{M}_1 = -\boldsymbol{K}\begin{bmatrix} \boldsymbol{M}_{v0}^{\mathrm{T}} & \boldsymbol{M}_{p0}^{\mathrm{T}} \end{bmatrix}^{\mathrm{T}} - \boldsymbol{R}_M\boldsymbol{F}_{p0} + \begin{bmatrix} \boldsymbol{0}_{1\times4} & c_T r_{vp} \end{bmatrix}^{\mathrm{T}} \tag{46}$$

$$\boldsymbol{R}_M = \begin{bmatrix} (\boldsymbol{R}_{vp}\boldsymbol{T}_{vp}^{\mathrm{T}})^{\mathrm{T}} & -k_T\begin{bmatrix} 0 & 0 & 1 \end{bmatrix}^{\mathrm{T}}\psi_{vp} \end{bmatrix}^{\mathrm{T}} \tag{47}$$

$$\boldsymbol{F}_{p0} = \boldsymbol{F}_{pAR} + \boldsymbol{F}_{pA\delta} + \boldsymbol{F}_{pG} \tag{48}$$

Equation (36) and (44) are simultaneously satisfied, so as to gain an eight DOF dynamic

equation of the flexible-wing aircraft:

$$\boldsymbol{E}\dot{\boldsymbol{x}} = -\boldsymbol{F} \tag{49}$$

where

$$\boldsymbol{E} = \begin{bmatrix} \boldsymbol{E}_F^{\mathrm{T}} \\ \boldsymbol{E}_M^{\mathrm{T}} \\ [\boldsymbol{0}_{4\times 8} \quad \boldsymbol{I}_4]^{\mathrm{T}} \end{bmatrix}, \quad \boldsymbol{F} = \begin{bmatrix} \boldsymbol{F}_1^{\mathrm{T}} \\ \boldsymbol{M}_1^{\mathrm{T}} \\ \boldsymbol{\omega}_{vp}^{\mathrm{T}} \\ p_p + \tan\theta_p (q_p \sin\phi_p + r_p \cos\phi_p) \\ q_p \cos\phi_p - r_p \sin\phi_p \end{bmatrix}.$$

3 Analysis of relative motion

In order to evaluate the validity of the dynamic model, the simulation experiment is carried out aiming at a small type of the flexible-wing aircraft. The relative motion characteristics are simulated and analyzed, such as turning, flare landing, and responses of thrust. The structural parameters of a small flexible-wing aircraft are shown as Table 1.

Table 1 Main specification of the flexible-wing aircraft

Parameter	Value
Span (b)	10.9m
Chord length c	2.8m
Parafoil area S_p	30 m^2
Aspect ratio (AR)	3.9
Cord length (l)	6.2m
Parafoil mass (m_p)	6.3kg
Payload mass (m_v)	90kg
Equivalent area of the payload (S_v)	0.75 m^2

The initial state of the flexible-wing aircraft is $\boldsymbol{V}_p^T = [15.6 \quad 0 \quad 0.4]^T$, $\boldsymbol{\omega}_p^T = \boldsymbol{0}_{3\times 1}$, $\boldsymbol{\omega}_{\mathrm{vp}}^T = [0.03 \quad 0]^T$, $[\theta_{vp} \quad \psi_{vp}]^T = [-5.5 \quad 0]^T$, $[\phi_p \quad \theta_p]^T = [0 \quad 15.1]^T$, the initial height is $Z = 980m$, and the initial thrust is $\boldsymbol{F}_{vth} = 248.7N$.

3.1 Response to thrust change

Calculation indicates the vehicle can level fight when $\boldsymbol{F}_{vth} = 248.7N$, and the thrust is a medium power at this time. Velocities of two bodies keep the same when the aircraft is gliding after the parafoil is inflated completely. The main effect of thrust reflects in the horizontal velocity, the vertical velocity and the pitch angle.

Fig. 3 shows the change curves of the horizontal and vertical velocity of the parafoil with different thrust. With the increase of thrust, the horizontal velocity increases toward the positive direction of X axis. The main effect reflects in the increase of the vertical velocity toward the negative direction of Z axis. That is because the attack angle of parafoil increases due to the thrust, which results in the increase of aerodynamic lift, and the increase of lift leads to the increase of the vertical velocity. $u_p = 18.6m/s$, $w_p = -2.2m/s$ when the maximum thrust is $\boldsymbol{F}_{vth} = 548.7N$.

Fig. 4 and Fig. 5 show the pitch angle, relative pitch angle and relative pitch rate. The thrust cause a large oscillation in the pitch angle, and two bodies have obvious relative motion. The maximum amplitude of relative pitch angle is about 20°. That is because the thrust act to the payload, the speed of response of payload is faster than the parafoil.

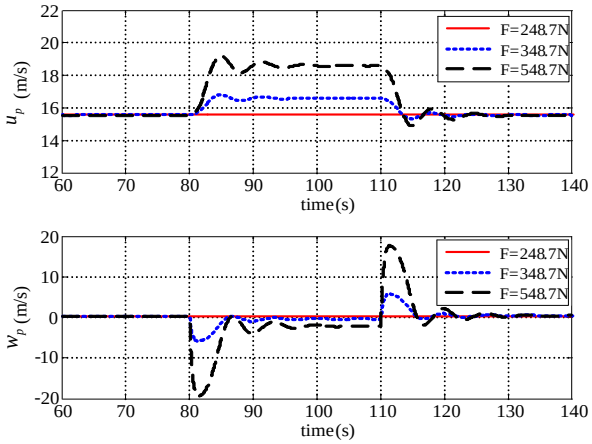

Fig. 3 Change curves of horizontal velocity and vertical velocity

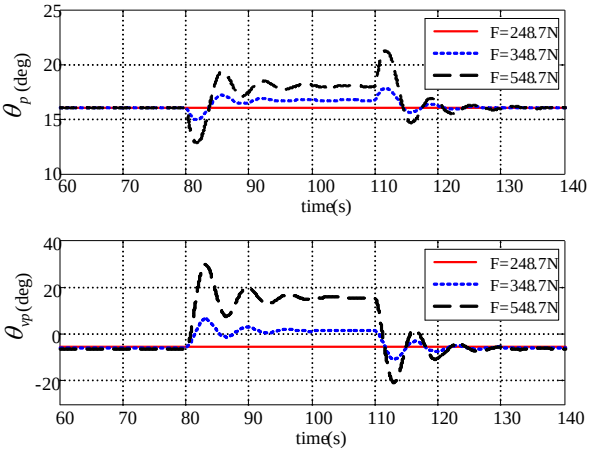

Fig. 4 Change Curves of pitch angle and relative pitch angle

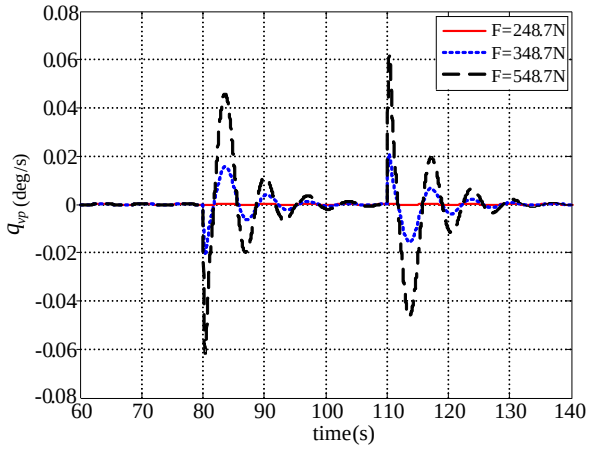

Fig. 5 Change curves of relative pitch rate

3.2 Motion of turning

At 50s, the left steering line on the trailing edge of parafoil is pulled down in varying deflection until 110s. The corresponding motion characteristics are shown as Figs. 6, 7 and 8.

Fig. 6 indicates the lateral velocity change, from which it can be seen that the lateral velocity increases with the increase of the deflection, and the maximum velocity is $v_p = -4\,\mathrm{m/s}$ when the deflection reaches 70%.

The yaw angle change in Fig. 7 indicates both of the yaw angle and the relative yaw angle of the parafoil are zero in the phase of gliding. After left steering lines is pulled down, the yaw angle increases linearly, and the relative yaw angle increases toward the positive direction and stabilizes at about 3.8° when the deflection is $\delta_r = 70\%$. The relative motion of two bodies is observed.

Fig. 8 shows trajectory of the vehicle in horizontal plane with different deflection. From Fig. 8, when pulling the left steering line, the vehicle turns left accordingly. The turning radius is inversely proportional to the deflection ($C_{30\%} = 93m$, $C_{50\%} = 67m$) and the stability becomes bad. It can be discovered that the relative motion and the oscillation of the attitude is over fierce when the deflection is $\delta_r \geq 70\%$, and damping of the oscillation is poor. Therefore, it is generally controlled within a safety range of $\delta_r \leq 50\%$ in actual operation.

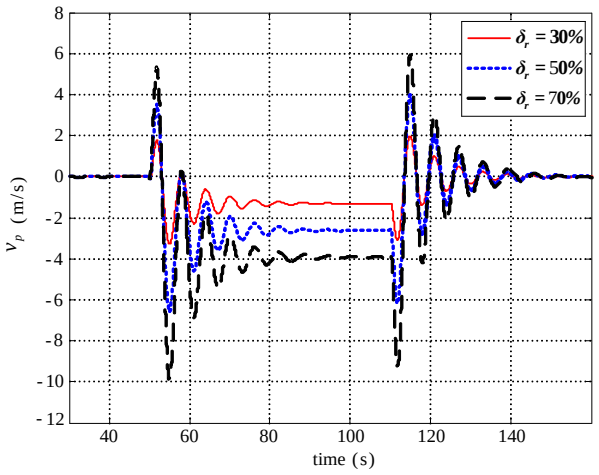

Fig. 6 Change curves of lateral velocities

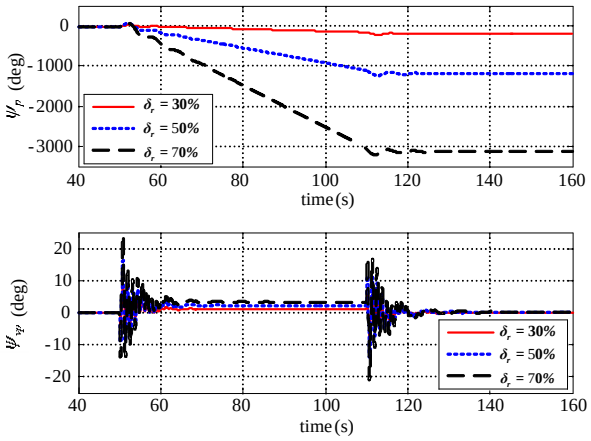

Fig. 7 Change curves of yaw angle and relative yaw angle

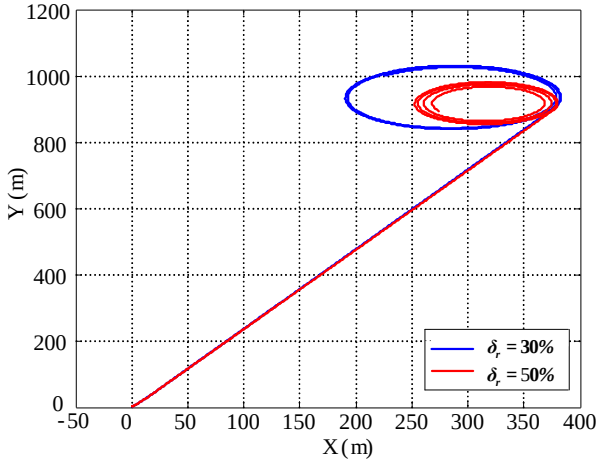

Fig. 8 Trajectory in horizontal plane

3.3 Motion of flare landing

The work condition is set as that 50s, the both steering lines on the trailing edge of parafoil are pulled down by the deflection variation simultaneously and quickly. The corresponding motion characteristics are shown as Figs. 9, 10 and11, and Fig. 12 shows the trajectory of the vehicle.

From the Figures, when the lines are pulled down quickly, the pitch angle and the relative pitch angle will oscillate, which results in oscillate of vertical velocity of vehicle. When $t = 51.5s$, the vertical velocity decreases to the minimum $0.51m/s$. Then the vertical velocity increases, and at last trend toward stabilization. So pulling down the both lines can realize the effect of speed reduction to the vehicle. If the time of maneuver is chosen appropriately, the vehicle will land just while the velocity decreases to the minimum value. This realizes flare landing. So, to achieve nondestructive landing, the timing of maneuver when landing is determined according to the practical working condition and the shock absorption measures.

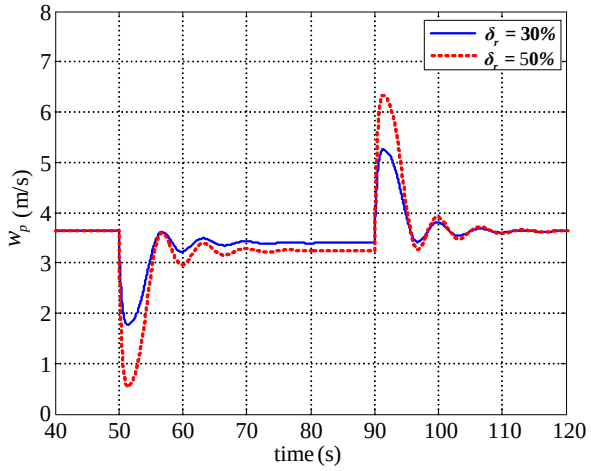

Fig. 9 Change curves of vertical velocity

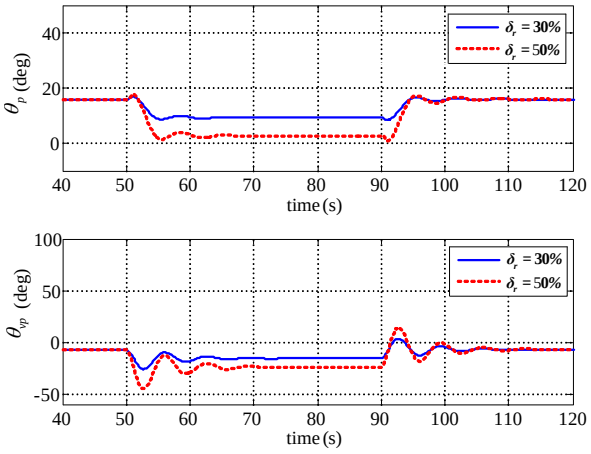

Fig. 10 Change curves of pitch angle and relative pitch angle

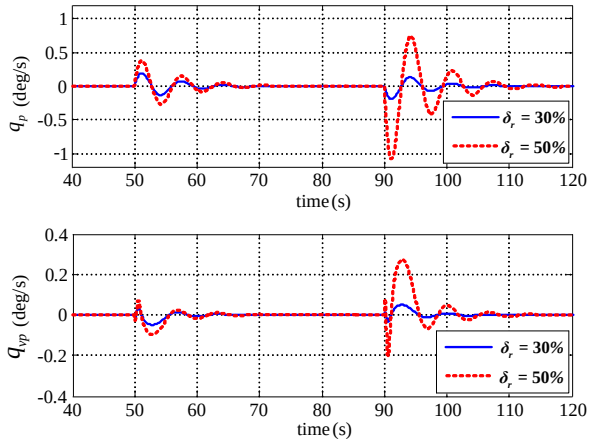

Fig.11 Change curves of pitch angle and relative pitch angle

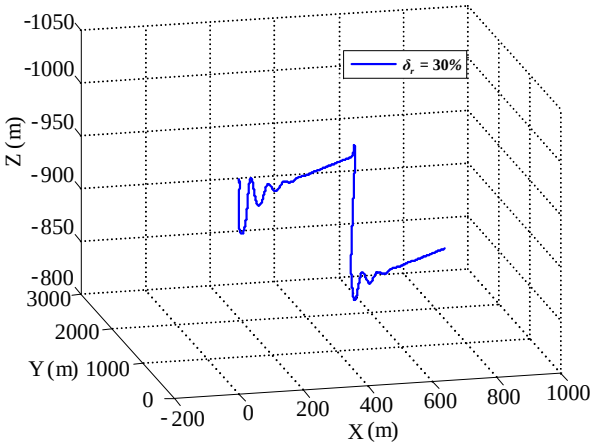

Fig. 12 Trajectory (3D)

4 Simulation of wind disturbances

Compared with the fixed-wing aircraft, the flight velocity of the flexible-wing aircraft is lower ($V_{\max}=18\mathrm{m}/s$) and the volume-to-mass ratio of parafoil is great. These characteristics of the flexible-wing aircraft make it subjective to wind disturbances, which may cause a significant oscillation as in the preceding section. Therefore, it is necessary to analyze its flight characteristics in the presence of wind disturbances.

As Fig. 13 shows, a spherical polar coordinate system $\Sigma_w(\mathrm{V}_w,\vartheta_w,\zeta_w)$ is employed to define the wind velocity and the direction, in which V_w means wind velocity, ϑ_w means elevation angle, and ζ_w means azimuth angle. $\boldsymbol{V}_{\mathbf{wu}}=\mathrm{V}_w[\sin\vartheta_w\cos\zeta_w \quad \sin\vartheta_w\cos\zeta_w \quad \cos\vartheta_w]^{\mathrm{T}}$ is defined as the wind vector in Σ_I, and the wind component is $\boldsymbol{V}_{wp}=\boldsymbol{T}_{Ip}\boldsymbol{V}_{wu}$ in Σ_p, in which $\boldsymbol{T}_{Ip}$ is the transformation matrix from Σ_I to Σ_p.

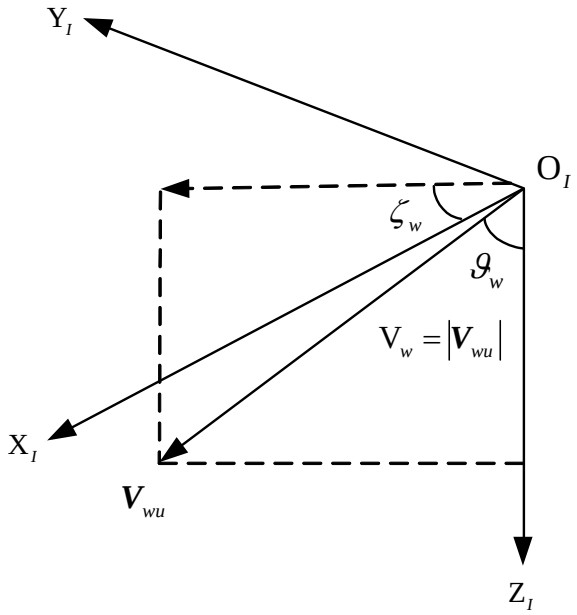

Fig. 13 Wind Coordinate System

4.1 Head wind disturbances in straight flight

In consideration of a straight level flight in head wind disturbances, the thrust is $\boldsymbol{F}_{vth}=248.7N$, and there are no left and right deflection ($\delta_{\mathrm{L}}=\delta_{\mathrm{R}}=0$). The disturbances is defined as head wind, the direction is $\vartheta_{\mathrm{W}}=\pi/2$, $\zeta_{\mathrm{W}}=0$, and the gust velocity is shown in Fig. 14.

Fig. 15 shows changes of pitch angles, from which it can be seen that, the oscillation of the pitch angle still exists in the two bodies although the two-body flexible connection features self-stabilization and the relative pitch plays a role of damping to some extent. The maximum oscillation amplitudes are $\theta_{\mathrm{p}}=6^{\circ}$ and $\theta_{\mathrm{v}}=8^{\circ}$, respectively, when the wind velocity is $\mathrm{V}_{\mathrm{W}}=3\mathrm{m}/\mathrm{s}$.

Fig. 16 shows the altitude change, in which the altitude oscillation is similar to the phugoid-mode of the fixed-wing aircraft, but the oscillation of the flexible-wing aircraft is due to the motion of pendulum which is caused by disturbances.

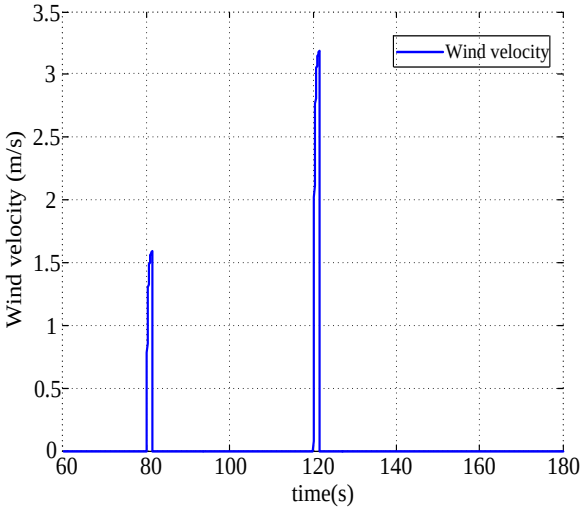

Fig. 14 Change curve of wind velocity

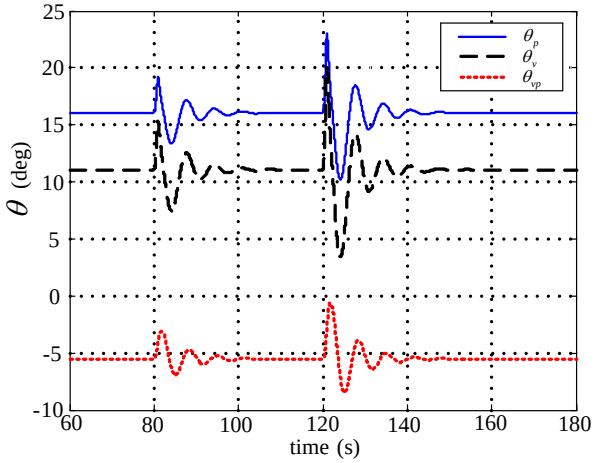

Fig. 15 Change curves of pitch angle

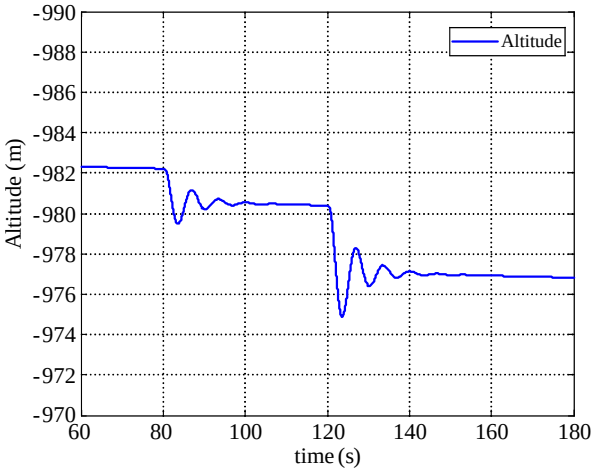

Fig. 16 Change curve of altitude

4.2 Head variable wind disturbances in straight flight

Head variable wind is defined as the disturbances. The Wind velocity and the direction changes are respectively shown in Fig. 17 and Fig. 18, in which the wind direction elevation is $\vartheta_W = \pi/2$ and the azimuth change is $\zeta_W = \pm 10^\circ$.

Fig. 19 shows time histories of the attitude angles. The large pitch oscillation occurs after the wind disturbance is input, and then, the variation of the wind direction causes the lateral-directional oscillations. Fig. 20 shows the trajectory of the vehicle in the horizontal plane, and lateral oscillation offset is caused by the variation of the wind direction, with the maximum oscillation of 1.6m.

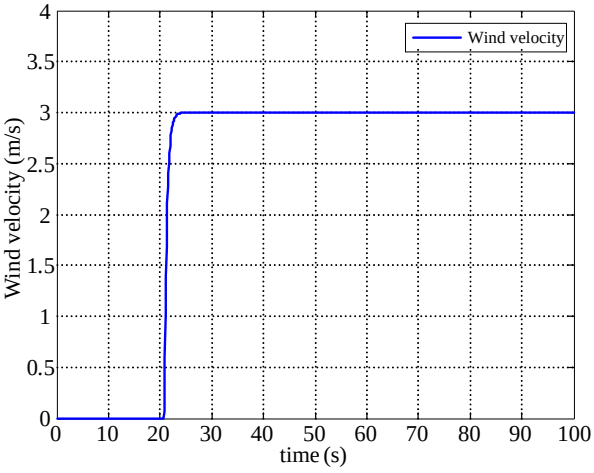

Fig. 17 Change curve of the wind velocity

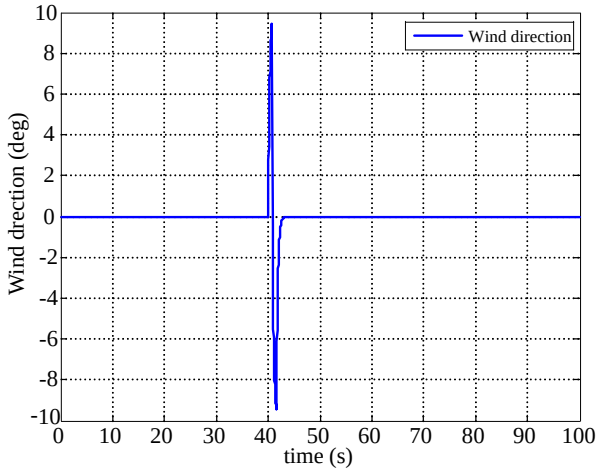

Fig. 18 Change curve of the wind direction

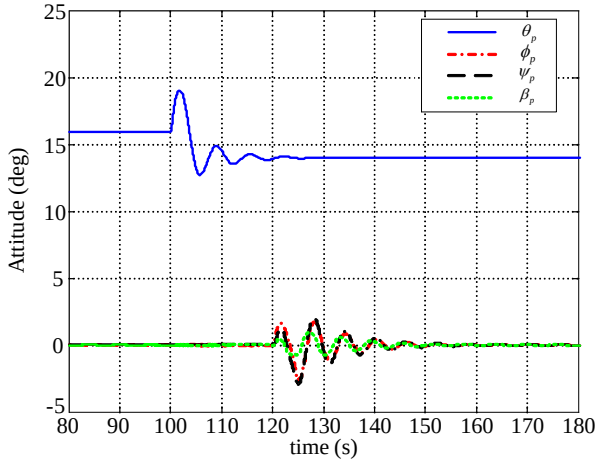

Fig. 19 Change curve of the attitude angles

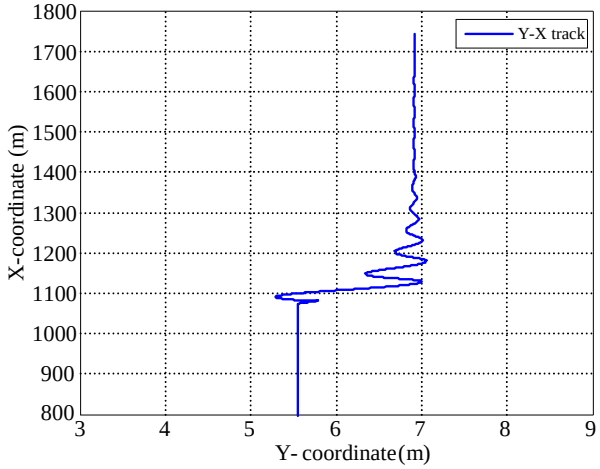

Fig. 20 Trajectory in horizontal plane

4.3 Left wind disturbances

In this case, the wind disturbance is given by the left side of the vehicle. The wind velocity at 120s in Fig. 14 is selected, and the wind direction comes from the left side of the vehicle ($\vartheta_W = \pi/2$, $\zeta_W = \pi/2$). Fig. 21 shows the attitude angles of the parafoil, from which the disturbance causes great oscillation in the yawing and rolling angles of the parafoil.

The maximum amplitudes of the yaw and roll angles are $\psi_p = 21^\circ$ and $\theta_p = 4^\circ$, and the periods of oscillation are 8s and 7s. The rolling and yawing motion is similar to the Dutch-roll mode of a fixed-wing aircraft. Fig. 22 shows the trajectory of the vehicle in the horizontal plane, in which the wind disturbance causes large lateral oscillation and the maximum amplitude is 19m at $X = 650\text{m}$.

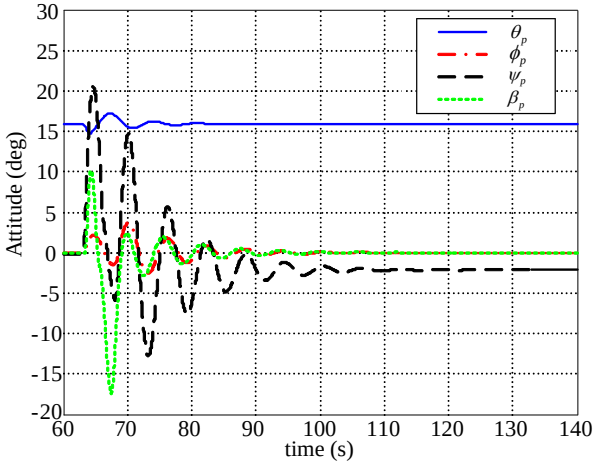

Fig. 21 Change curve of the attitude angles

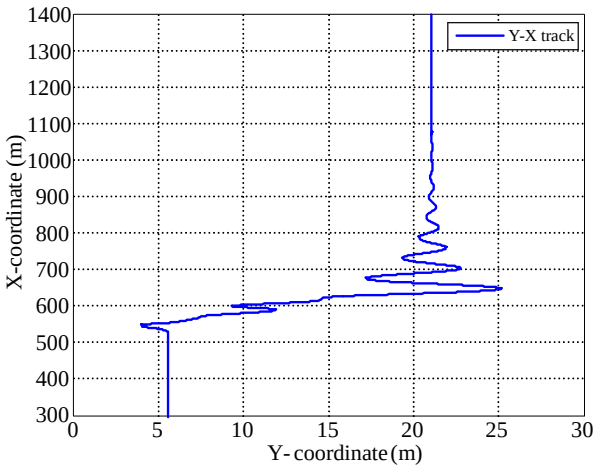

Fig. 22 Trajectory in horizontal plane

4.4 Wind disturbances during right-turn

Wind disturbances during the right-turn level flight is considered, the wind velocity at 120s in Fig. 14 is selected, and the wind direction is $\vartheta_W = \pi/2$, $\zeta_W = 0$. The applied control input are as follows: $\boldsymbol{F}_{vth} = 248.7N$, $\delta_R = 0.3$, $\delta_L = 0$.

Fig. 23 shows the attitude angles of the parafoil. The damping of the attitude oscillation is very poor. Fig. 24 shows the trajectory (3D) of the vehicle and it can be seen that the attitude angles oscillation caused by wind disturbances is also observed.

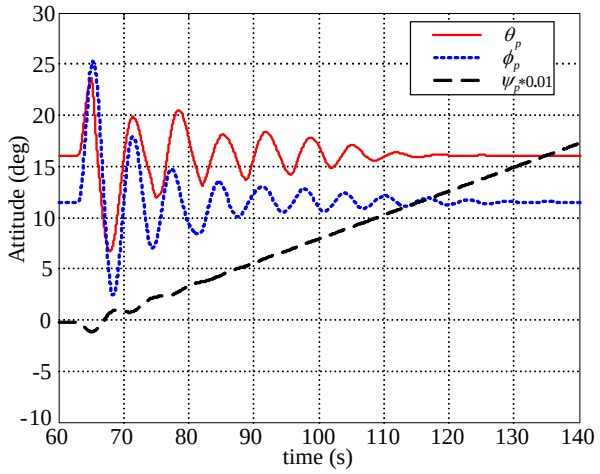

Fig. 23 Change curve of the attitude angles

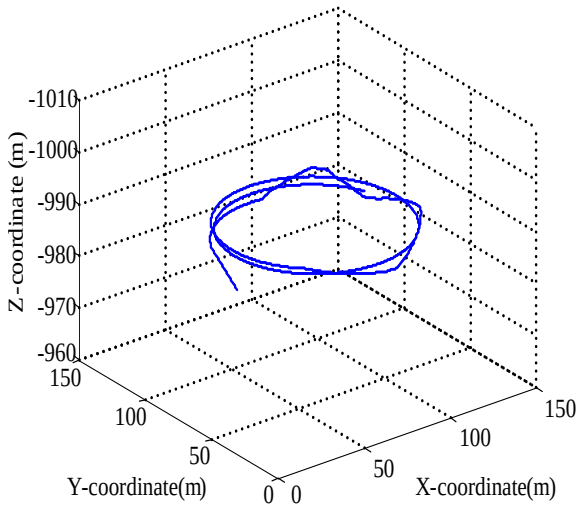

Fig. 24 Trajectory (3D)

5 Conclusion

The following researches on nonlinear modeling and motion characteristics against the multi-body structure and multi-degrees of freedom of the flexible-wing aircraft are conducted in this Paper: first, a mechanism method is used to build an eight DOF nonlinear dynamic model of the flexible-wing aircraft, in which apparent mass of the parafoil, relative motion between two bodies, and engine thrust are considered, and the eight DOF includes two DOF of two-body relative pitch and relative yaw except the parafoil's six DOF. Two-body connection way and tension of suspension lines are considered in force analysis, conforming to actual structure characteristics, the modeling process is relatively detailed, which provides the theory reference for the research on control strategy; second, the relative motion characteristics of gliding, turning of pulling single line, flare landing of pulling bilateral lines symmetrically, and responses of power and wind were analyzed by simulation, and some motion law of the flexible-wing aircraft was obtained. The simulation results verified the validity of the established model.

However, what is noteworthy is that: 1) the influence of random wind disturbances on the flight state of the vehicle is not considered; 2) different connection mode between the lines and payload has influence on the modeling, and the control mode of steering line, such as pull-down speed, should be considered; 3) the time delay in actual control response is still not considered in the model, which will have some influence on future research on control strategy. Therefore, the future

research will focus on model improvement and experimental verification.

Acknowledgement

This project is supported by the National Natural Science Foundation of China under Grant No. 51175508 and the Key Project of Innovation Engineering of GAD Colleges under Grant No. ZYX12080007.

References

[1] Smith, J., Bennett, T., and Fox, R.:Development of the Parafoil Landing System[R]. *AIAA-1730*, 2009.

[2] Goodrick, T.: Comparision of simulation and experi-mental data for a gliding parachut in dynamic[R], *AIAA-1924*,1981.

[3] Barrows, T.: Apparent mass of parafoil with spanwise camber[J]. *Journal of Aircraft*, ,Vol.39, No.3, 2002, pp. 445-451.

[4] Slegers, N.: Optimal Control for Terminal Guidance of Autonomous Parafoils[R]: *AIAA-2058*, 2009.

[5] Slegers, N, Costello, M.:Model predictive control of a parafoil and payload system[J]. *Journal of Gaidance Control and Dynamics*, Vol. 28, No.4, 2005, pp: 816-821.

[6] Heise, M., Muller, S.: Dynamic modeling and xisualization of multi-body flexible system[R]: *AIAA-4809*, 2004.

[7] Xiong, J.: Research on Dynamics and Homing Plan of Parafoil [D]. *Changsha: Doctoral Dissertation of National University of Defense Technology*, 2006

[8] Slegers, N.: Effects of canopy-payload relative motion on control of autonomous parafoils[J]. *Journal of Gaidance Control and Dynamics*, Vol.33, No.1, 2010, pp: 116-125.

[9] Ward, M., Costello, M.: Parametric study of powered parafoil flight dynamics[R]: *AIAA-4726*, 2012.

[10] Aoustin, Y., Martinenko, Y.: Control algorithms of the longitude motion of the powered paraglider[C]. In: *Proceedings of the Biennial Conference on Engineering Systems Design and Analysis*, 2012, PP. 775-784.

[11] Song, L., Yang, H., Liu, C.: Study on powered-parafoil longitudinal flight performance with a fast estimation model[J]. *Journal of Aircraft*, Vol.50, No.5, 2013, pp: 1660-1667.

[12] Ochi, Y.: Modeling and Simulation of Nonlinear Dynamics of a powered paraglider[R]: *AIAA-7418*, 2008.

[13] Ochi, Y.: Linear dynamics and PID flight control of a Powered Paraglider[J]. *Journal of Gaidance Control and Dynamics*, Vol. 32, No.3, 2010, pp: 78-89.

[14] Lissaman, P., Brown, G.: Apparent mass effects on parafoil dynamics[R]. *AIAA-1236*,1993.

[15] Goodrick, T.: Simulation studied of the flight dynamics of gliding parachute systems[R]. *AIAA-0417*, 1979.

[16] Yan, J., Gu, Z.: Microprocessor Controlling of Servo Mechanism (Single Motor) in Controllable Ram-Air Parachute[J]. *Spacecraft Recovery & Remote Sensing*, Vol.17 , No.2, 1996, pp: 17-21.